Environmental Science & Technology

Article

pubs.acs.org/est

Analysis of the Mo Speciation in the JEB Tailings Management Facility at McClean Lake, Saskatchewan

John R. Hayes,[†] Andrew P. Grosvenor,*[,†] John Rowson,[‡] Kebbi Hughes,[‡] Ryan A. Frey,[‡] and Joel Reid[§]

[†]Department of Chemistry, University of Saskatchewan, Saskatoon, Saskatchewan S7N 5C9, Canada

[‡]AREVA Resources Canada, Saskatoon, Saskatchewan S7K 3X5, Canada

[§]Canadian Light Source, Saskatoon, Saskatchewan S7N 2V3, Canada

Supporting Information

ABSTRACT: The JEB Tailings Management Facility (TMF) is central to reducing the environmental impact of the uranium ore processing operation located at the McClean Lake facility and operated by AREVA Resources Canada (AREVA). The geochemical controls of this facility are largely designed around the idea that elements of concern, such as Mo, will be controlled in the very long term through equilibrium with supporting minerals. However, these systems are far from equilibrium when the tailings are first placed in the TMF, and it can take years, decades, or centuries to reach equilibrium. Therefore, it is necessary to understand how these reactions evolve toward an equilibrium state to understand the very long-term behavior of the TMF and to ensure that the elements of concern will be adequately contained. To this end, the Mo speciation in a series of samples taken from the JEB TMF during the 2008 sampling campaign has been analyzed. This analysis was performed using powder X-ray diffraction (XRD), X-ray fluorescence mapping (μ-XRF), and X-ray absorption near-edge spectroscopy (XANES). These results show that only XANES was effective in speciating Mo in the tailings samples, because it was both element-specific and sensitive enough to detect the low concentrations of Mo present. These results show that the predominant Mo-bearing phases present in the TMF are powellite, ferrimolybdite, and molybdate adsorbed on ferrihydrite.

1. INTRODUCTION

The JEB Tailings Management Facility (TMF) is central to reducing the environmental impact of AREVA Resources Canada's (AREVA) uranium ore processing operations at the McClean Lake facility in northern Saskatchewan, Canada. Ultimately, geochemical control of solute concentrations in the JEB TMF, like many other TMFs around the world, will be provided over the long term through equilibrium with supporting minerals. The placed tailings are generally heterogeneous, and at the time of deposition into the TMF, the initial solute concentrations are generally out of equilibrium with their respective solids. Once the tailings are placed in the TMF, the solutes and mineralogy will gradually evolve toward a stable mineralogical end point. This evolution is slow (i.e., years, decades, or centuries) and generally limited by low hydraulic conductivity, low temperature (~6 °C), and low liquid/solid ratios that limit mass transport.[1] As part of its operating license issued by the Canadian Nuclear Safety Commission, it is incumbent upon AREVA to determine the minerals controlling the long-term pore water concentration of several elements of concern. These elements of concern are often co-mineralized with U in the ore body and include As, Ni, Mo, and Se in addition to U and ^{226}Ra. Mineralogical investigations by AREVA concerning several of these elements have been in progress for over a decade.[2−6] However, little work has been performed to determine the Mo-bearing minerals present.[1] In concordance with AREVA's operating requirements, it is prudent to ascertain what Mo-bearing phases are currently present in the TMF and how these phases evolve over time.

During the tailings preparation process, Mo is precipitated out of the solution component of the tailings slurry at a pH of 4 as ferrimolybdite [$Fe_2(MoO_4)_3{\cdot}8H_2O$] and molybdate adsorbed on ferrihydrite [$Fe(OH)_3$−MoO_4]. However, under the near-neutral TMF conditions unique to the JEB TMF (pH 7.3), these species are not stable and should dissolve, resulting in the formation of a new, relatively insoluble Mo-bearing phase. The geochemical models of the JEB TMF, which were based on thermodynamic calculations, predict that powellite ($CaMoO_4$) should precipitate in the TMF and control the Mo pore water concentration.[7] This is in contrast to another northern Saskatchewan TMF, which is operated at a higher pH, where $NiMoO_4$ or molybdate adsorbed on ferrihydrite have been identified as the prominent Mo species currently present.[8] It is necessary to experimentally determine if powellite is

Received: November 10, 2013
Revised: March 16, 2014
Accepted: March 25, 2014
Published: March 25, 2014

dx.doi.org/10.1021/es404980x | Environ. Sci. Technol. 2014, 48, 4460−4467

currently present in the JEB TMF to help verify the geochemical model. Further, it is also necessary to establish what other Mo-bearing phases are in the TMF and to understand how the Mo mineralogy in the TMF evolves over time. Such a study will help establish how the solubility of Mo will change over the very long term in a TMF with near-neutral pH.

To this end, the Mo speciation in several tailings samples from the 2008 sampling campaign was analyzed. AREVA conducts a sampling campaign of the TMF once every 5 years, and each campaign acts as a snapshot in time. The collective results will allow for an understanding of how these various equilibria processes evolve over time.[1] The Mo concentrations in the samples studied here range from 20 to 409 ppm (see Table S1 of the Supporting Information). Powder X-ray diffraction (XRD), X-ray fluorescence mapping (μ-XRF), and X-ray absorption near-edge spectroscopy (XANES) were used to analyze the Mo species present in the tailings. On the basis of this study, it can be concluded that powellite is present in the TMF and that it currently accounts for 10−40% of the Mo species in the JEB TMF. This result will aid future modeling of the JEB TMF as well as other TMFs. This study also found that the balance of the Mo was present as ferrimolybdite [$Fe_2(MoO_4)_3{\cdot}8H_2O$] and molybdate adsorbed on ferrihydrite [$Fe(OH)_3$−MoO_4]. Additionally, the effectiveness of several common techniques used in speciating low-concentration elements is also discussed. This investigation showed that only XANES was effective in determining the Mo species present because of the low Mo concentration and highly complex nature of the tailings samples.

2. EXPERIMENTAL SECTION

2.1. Mine Tailing Sample Selection. The samples used in this study were collected during the 2008 sampling of the JEB TMF. In these studies, drilling was conducted at four different locations around the TMF, and samples were collected at 3 m vertical intervals. The samples studied here were collected from two drilling positions, TMF08-01 (N 112.00°, E 52.89°), which is in the center of the TMF, and TMF08-03 (N 112.22°, E 52.39°), which is located at the periphery of the TMF. Three samples from each position were analyzed, and these are labeled as TMF08-01 SA04, TMF08-01 SA09, TMF08-01 SA19, TMF08-03 SA02, TMF08-03 SA08, and TMF08-03 SA16, where increasing SA numbers indicate deeper sampling depths. The depths of the samples used in this study are reported in Table S1 of the Supporting Information. In general, because of the deposition process of tailings within the TMF, coarser particles were expected to be found near the center of the TMF and finer particles were expected to be found at the periphery. Because of the settled nature of the TMF, the depth of the core sample can be correlated to the sample age, allowing for an analysis of the aging process of the tailings.

2.2. Preparation of Standard Materials. A series of Mo-bearing standards were either prepared or purchased to allow for analysis of the Mo speciation via Mo K-edge XANES experiments. These standards were chosen on the basis of a previous study of the Mo content of the DTMF operated by the Cameco Corporation.[8] The purchased standards were MoO_3 (Acrôs Organics, 99+%), MoS_2 (Aldrich), MoO_2 (Alpha Aesar, 99%), and H_2MoO_4 (Sigma Aldrich, >85%). The synthesized standards were powellite ($CaMoO_4$), α-$NiMoO_4$, α-$FeMoO_4$, ferrimolybdite [$Fe_2(MoO_4)_3$], and MoO_4^{2-} adsorbed on ferrihydrite [$Fe(OH)_3$−MoO_4]. The details of the synthetic methods used are presented in the Supporting Information.[8−13] The phase purity of all of the synthesized standards was checked by XRD using the instrument described in section 2.3.

2.3. Powder XRD. Powder XRD patterns from the tailings samples were collected to make an initial assessment of the phases present in these materials. Measurements were collected using a PANalytical Empyrean X-ray diffractometer equipped with a Cu K$\alpha_{1,2}$ X-ray source. The μ-XRD diffraction patterns were collected using a 200 μm diameter spot size. The details of the sample preparation and experimental setup are outlined in the Supporting Information. All powder XRD patterns were analyzed using the X'Pert HighScore Plus and PowderCell software packages.[14]

2.4. X-ray Fluorescence Imaging and Laue Diffraction. X-ray fluorescence (XRF) maps and Laue XRD patterns from three of the tailings samples were collected using the VESPERS beamline at the Canadian Light Source (CLS). (μ-XRD experiments were also attempted using multiple incident energies, but the collected signal was not high enough to produce a usable diffraction pattern.) Details of the sample preparation and experimental setup are presented in the Supporting Information. Fluorescence (elemental) maps were created and analyzed using the SMAK program, and the Laue diffraction patterns were analyzed using the XMAS program.[15,16]

2.5. XANES. Mo K-edge XANES measurements were carried out using the HXMA beamline at the CLS.[17,18] The details of the sample preparation and experimental setup are presented in the Supporting Information. In all cases, multiple scans of each sample were collected at a single spot. These scans did not change in any systematic way, indicating that no beam damage occurred during the measurements. The spectra were fitted from 25 eV below the absorption edge to 55 eV above the absorption edge when performing the principle component analysis (PCA) and linear combination fitting (LCF). The absorption edge of a spectrum was defined as the most intense, lowest energy peak in the first derivative of the spectrum. The Athena software program was used to normalize the spectra and perform all of the PCA and LCF analyses.[19]

3. RESULTS AND DISCUSSION

3.1. Powder XRD. Powder XRD patterns from the bulk tailings samples were collected to provide an initial characterization of the tailings materials (see Figure S1 of the Supporting Information). The dominant crystalline phases observed in these samples were quartz and gypsum. In general, the patterns from the central bore-hole samples (TMF08-01 SA04, TMF08-01 SA09, and TMF08-01 SA19; see Figure S1a of the Supporting Information) have a flatter background than the patterns from the periphery bore-hole samples (TMF08-03 SA02, TMF08-03 SA08, and TMF08-03 SA16; see Figure S1b of the Supporting Information), which contain a broad peak spanning ∼15−30°. This indicates that the samples from the central bore hole are more crystalline than the samples from the periphery bore hole.[20] This is consistent with the design of the TMF, because coarser particles are expected to congregate near the center of the TMF, while finer particles are expected to be found toward the edge of the TMF. Finally, the powder patterns show that none of the expected crystalline Mo-bearing phases (i.e., α-$FeMoO_4$, α-$NiMoO_4$, and powellite) could be detected using bulk powder XRD. This result was expected given the low concentrations of Mo in these samples (see Table

dx.doi.org/10.1021/es404980x | Environ. Sci. Technol. 2014, 48, 4460−4467

S1 of the Supporting Information) but does not preclude the presence of these phases in the tailings samples.

Given the limitations of a standard powder XRD experiment, these studies were followed by performing μ-XRD experiments. The X-ray beam was focused to a 200 μm spot size in these studies, and diffraction patterns were gathered from multiple aliquots of each sample. The results from sample TMF08-03 SA08 are presented in Figure 1 (the μ-XRD patterns from the other tailings samples are presented in Figures S2−S6 of the Supporting Information). The significant variations in the diffraction patterns observed indicate that the tailings samples are heterogeneous, which was also confirmed by visual inspection (photographs of two of the tailings samples are presented in Figure S7 of the Supporting Information). Additionally, the peak widths of the μ-XRD patterns vary, indicating that the crystallinity of the tailings is not uniform. Here, diffraction patterns with sharper peaks indicate a more crystalline sample. In general, the peaks can be assigned to phases previously reported to be found in the samples.[1] Interestingly, the intensities of peaks from highly crystalline phases varied significantly between samples (cf. scans 3 and 5 in Figure 1). These intensities also deviated significantly from the reported standard diffraction pattern. It is likely that these variations occur because of poor crystallite statistics ("graininess"), in which the crystallites are sufficiently large that too few grains are illuminated to obtain a statistically representative distribution of grain orientations, resulting in a random distortion of the diffraction peak intensities.[21] This seems likely given the large grain sizes (the samples were not ground) and the small X-ray spot size. These patterns provide some possible evidence for the presence of β-$FeMoO_4$ and powellite phases. However, for powellite, the predominant peak observed is not the most intense peak in the reported reference pattern, suggesting that graininess is likely an issue here as well. Overall, these results show that a more sophisticated approach is required to determine the Mo speciation in these tailings samples.

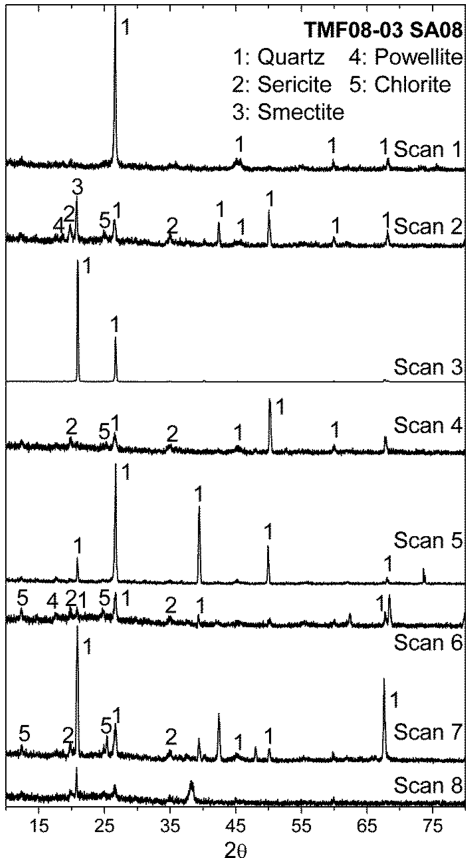

Figure 1. μ-XRD patterns collected from aliquots of the TMF08-03 SA08 tailings sample. The diameter of the beam spot was 200 μm. In some scans, the intensities of the identified peaks do not match the calculated intensity from the reference pattern. This is most notably seen for the quartz peaks in scans 3 and 7 and is likely caused by graininess of the crystallites. A peak consistent with the presence of powellite is found in scans 2 and 6.

3.2. XRF Imaging and Laue Diffraction. *3.2.1. XRF Imaging.* XRF experiments were performed to map the elemental distribution within the tailings samples. In these experiments, the samples were illuminated with a highly focused X-ray pink beam, which had a spot size of 5 μm. The samples were then rastered using 10 μm steps, and the resulting fluorescence at each spot was measured, allowing for a map to be generated. The results of this experiment for the TMF08-03 SA08 sample are shown in Figure 2. Two other tailings samples were also mapped (see Figures S8 and S9 of the Supporting Information), but Mo could not be detected in the regions studied.

A Mo-rich region was observed near the bottom left-hand corner of the map, as outlined by the red rectangle in Figure 2. Relatively intense fluorescence signals from U, As, Ni, and Fe were also observed in this region. The size and shape of these hotspots were similar, suggesting that these elements are intimately mixed with Mo. There was little overlap between the Ca- and Mo-rich regions, although some small, isolated Ca hotspots were observed to overlap with the main Mo hotspot. A strong correlation between the U and Mo signals was observed, which may indicate that U and Mo are present in a single phase. However, it is more likely that this result is an artifact of the relatively poor resolution of the fluorescence detector. The Mo Kα emission line has an energy of 17 480 eV, and the U Lβ emission line has an energy of 17 220 eV. It is possible that the overlap between signal channels resulted in this correlation.[18] In general, these results may indicate that Ni and Mo are intimately mixed, consistent with the presence of a $NiMoO_4$ phase, but it is more likely that this observation was a result of the co-mineralization of Ni- and Mo-bearing phases from the original ore. Overall, no conclusive results about the Mo speciation could be drawn from this experiment.

3.2.2. Laue Diffraction. Laue diffraction patterns were collected at different sample positions based on the results of the XRF mapping experiments. The positions at which patterns were collected are labeled in Figure 2 and Figures S8 and S9 of the Supporting Information, on the As fluorescence maps. The samples were illuminated using an X-ray pink beam with a spot size of 5 μm in these experiments. Representative examples of the patterns collected are presented in Figure 3.

The spot size used (5 × 5 μm) was on the order of the size of the crystallites, and the resulting diffraction patterns collected generally resemble single-crystal diffraction patterns. This is observed best in the pattern presented in Figure 3b, in which small, well-defined diffraction spots are observed. However, the significant penetration depth of the X-rays can also result in several crystallites being illuminated simultaneously, resulting in large, non-circular diffraction spots (see panels a and c of Figure 3).

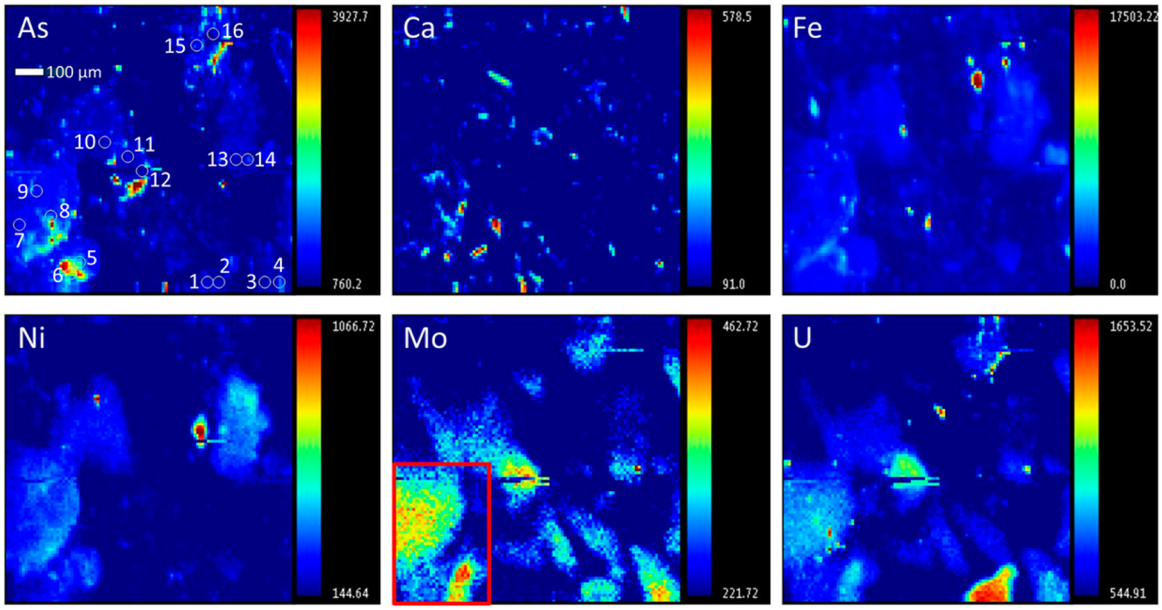

Figure 2. Fluorescence maps collected from the TMF08-03 SA08 sample. The spot size of the beam was 5 × 5 μm, and the map was collected using 10 μm steps. The spots where Laue diffraction patterns were collected are labeled according to their scan number in the As map. A large Mo concentration hotspot was found in the lower left-hand corner of the Mo map, as outlined by the red rectangle. Fe, Ni, As, and U fluorescence signals were also observed in this region, indicating that these elements were likely intimately mixed.

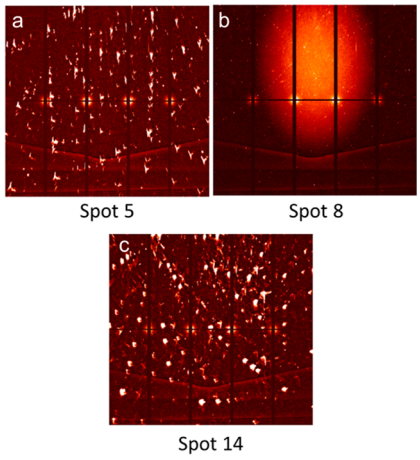

Figure 3. Laue diffraction patterns collected at (a) spot 5, (b) spot 8, and (c) spot 13 from the TMF08-03 SA08 tailings sample. The spot size of the beam was 5 × 5 μm. The "V shape" present in the bottom half of the patterns is the result of shadowing from the sample holder. The diffraction patterns collected at spots 5 and 14 are broad and non-circular, indicating that multiple crystallites were illuminated. The diffraction pattern collected at spot 8 is small and circular, indicating that only one crystallite was illuminated.

These patterns were analyzed using the crystal structure of known standards to index the diffraction spots. If the number of diffraction spots indexed was close to the number of diffraction spots observed, it is likely that the phase indexed is present.[22] Here, the phases indexed were those reported by AREVA to be in the tailings. The results of these fitting attempts are summarized in Table 1 and Tables S2 and S3 of the Supporting Information (note that some spots did not produce usable diffraction patterns). In general, none of the phases indexed resulted in a definitive fit. However, for TMF08-03 SA08, spot 8 may have been indexed by powellite and the diffraction pattern of spot 6 was modeled fairly well by gypsum. Ultimately, the complexity of the tailings samples did not allow for any conclusions to be drawn.

3.3. XANES. Mo K-edge XANES spectra from the tailings samples and a series of Mo-bearing standards were collected and are presented in Figure 4. The spectra were analyzed to determine the speciation of Mo in the tailings samples. The results of this analysis are discussed below.

3.3.1. Analysis of the Mo Oxidation State in the Tailings. The Mo K-edge XANES spectra were first analyzed to determine the oxidation state of Mo in the tailings species. This analysis was performed by comparing the absorption edge energies of spectra from the tailings samples to spectra from samples with known Mo oxidation states (Figure 5). The absorption edge energy is sensitive to the oxidation state of the metal center, and the absorption edge shifts to higher energy with increasing oxidation state. Increasing the oxidation state decreases the amount of screening of the nuclear charge that the core−electron experiences, leading to a more tightly bound ground state.[23,24] The edge energy is also sensitive to the chemical environment around the metal center, because changes in the electronegativity of the surrounding anions can change the bond covalency. In general, as the surrounding ions become less electronegative (i.e., the bonds become more covalent), the charge of the Mo center decreases and the absorption edge energy shifts to lower energy.[23,24] This is best observed by comparing the edge energies of MoO_3 (Mo^{6+}), MoO_2 (Mo^{4+}), and MoS_2 ($Mo^{4-\delta+}$) in Figure 5; as the Mo oxidation state decreases, the edge energy also decreases. Examination of Figure 6 shows that the absorption edge energies from the tailings samples are similar to the absorption edge energy from MoO_3. It can be concluded that Mo adopts a 6+ oxidation state in the tailings samples and is likely surrounded by O anions. This is consistent with the processing of the tailings, in which a large amount of Fe^{3+} is added to the mixture, because it is well-known that the $Fe^{3+}/Mo^{4/5+}$ redox couple strongly favors the formation of Fe^{2+} and Mo^{6+} under a wide variety of conditions.[25,26]

dx.doi.org/10.1021/es404980x | Environ. Sci. Technol. 2014, 48, 4460−4467

Table 1. Summary of Laue Fitting Results, TMF08-03 SA08

	number of peaks indexed[a]						
image[b]	powellite	quartz	illite−smectite	chlorite	gypsum	kamiokite	β-$FeMoO_4$
1	34	43	42	49	46	29	126
2	47	49	36	43	46	45	147
6	19	12	15	15	29	18	48
8	56	56	48	54	58	54	175
11	55	43	43	27	39	43	149
13	43	31	28	27	41	27	97
14	35	40	31	42	45	40	131
15	35	42	41	60	40	41	156
16	43	67	42	49	52	40	162

[a]Larger numbers of peaks indexed usually indicate a higher quality fit.[22] [b]Numbering refers to where on the sample the diffraction pattern was collected. Please refer to Figure 2 for image locations.

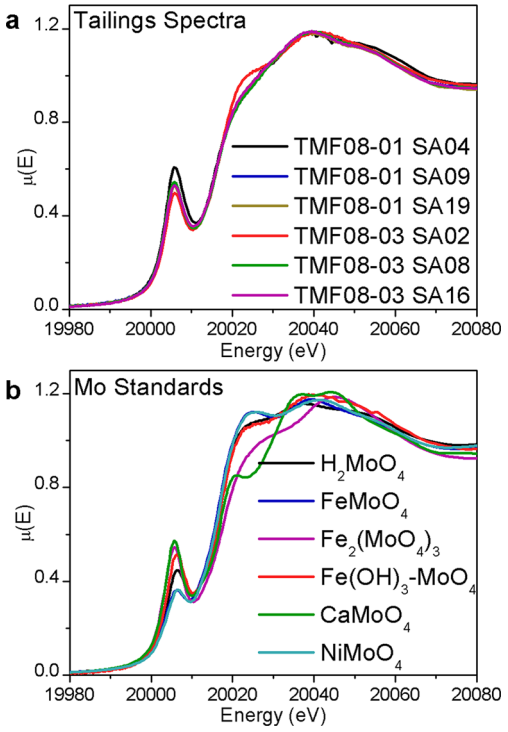

Figure 4. (a) Mo K-edge XANES spectra from the tailings samples. All spectra were fairly similar, with the exception of the spectrum collected from the TMF08-03 SA02 sample. (b) Mo K-edge XANES spectra from the Mo standards used for the linear combination fitting.

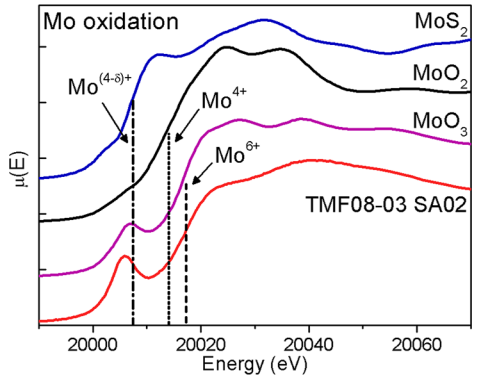

Figure 5. Absorption edge energy of the TMF08-03 SA02 sample is compared to Mo standards with different oxidation states. The absorption edge energy is similar to that from MoO_3, which has a 6+ oxidation state, indicating that Mo likely adopts a 6+ oxidation state and is surrounded by O^{2-} anions in the tailings samples.

3.3.2. PCA. Beyond information on the oxidation state and the local coordination environment around the metal center, XANES can also provide information about the number of species present in a mixture and the identity of those species. Such information is achieved through the use of advanced data processing techniques, such as PCA. In this context, the term "component" and the term "factor" are interchangeable. To avoid the confusion of trying to refer to both chemical and mathematical components, the term "factor" will be used when describing PCA components. The basic principle of PCA (in the context of XANES) is grounded in the fact that a XANES spectrum from a mixture can be constructed from a linear combination of the spectra from each of the individual components in that mixture.[27] Because of this property, the spectra from a series of mixtures bearing similar individual components can be decomposed into q principle factors, which can be used to reconstruct the original data.[28] PCA has been performed on the set of tailings spectra investigated here, and the results of this analysis are plotted in Figure S10 of the Supporting Information. It is important to note that, despite their appearance, the principle factors derived from the data are mathematical constructs and do not have physical meaning. The analysis of the spectra reported here is similar to the analysis used to determine the Mo species present in the DTMF, which is a U-milling TMF also located in northern Saskatchewan.[8]

Given a perfect data set with no experimental error, the number of principle factors would be equal to the number of components within the set of mixtures. However, the number of principle factors derived is always greater than the number of components in the set of mixtures because of experimental error.[28] In this case, the excess principle factors describe the contributions of experimental error to the data. The principle factors attributable to the components within the set of mixtures are referred to as primary factors, while principle factors attributable to experimental error are referred to as secondary factors. Malinowski has developed the empirical IND function to differentiate between the primary and secondary factors, and the number of primary factors is given when the IND function output is minimized.[28,29] The values of the IND function have been evaluated and are plotted in Figure S11 of the Supporting Information. The IND function reached a minimum value when the number of principle factors was 3. It was concluded from this analysis that there are three Mo-bearing species in the tailings. This conclusion is confirmed by

dx.doi.org/10.1021/es404980x | Environ. Sci. Technol. 2014, 48, 4460−4467

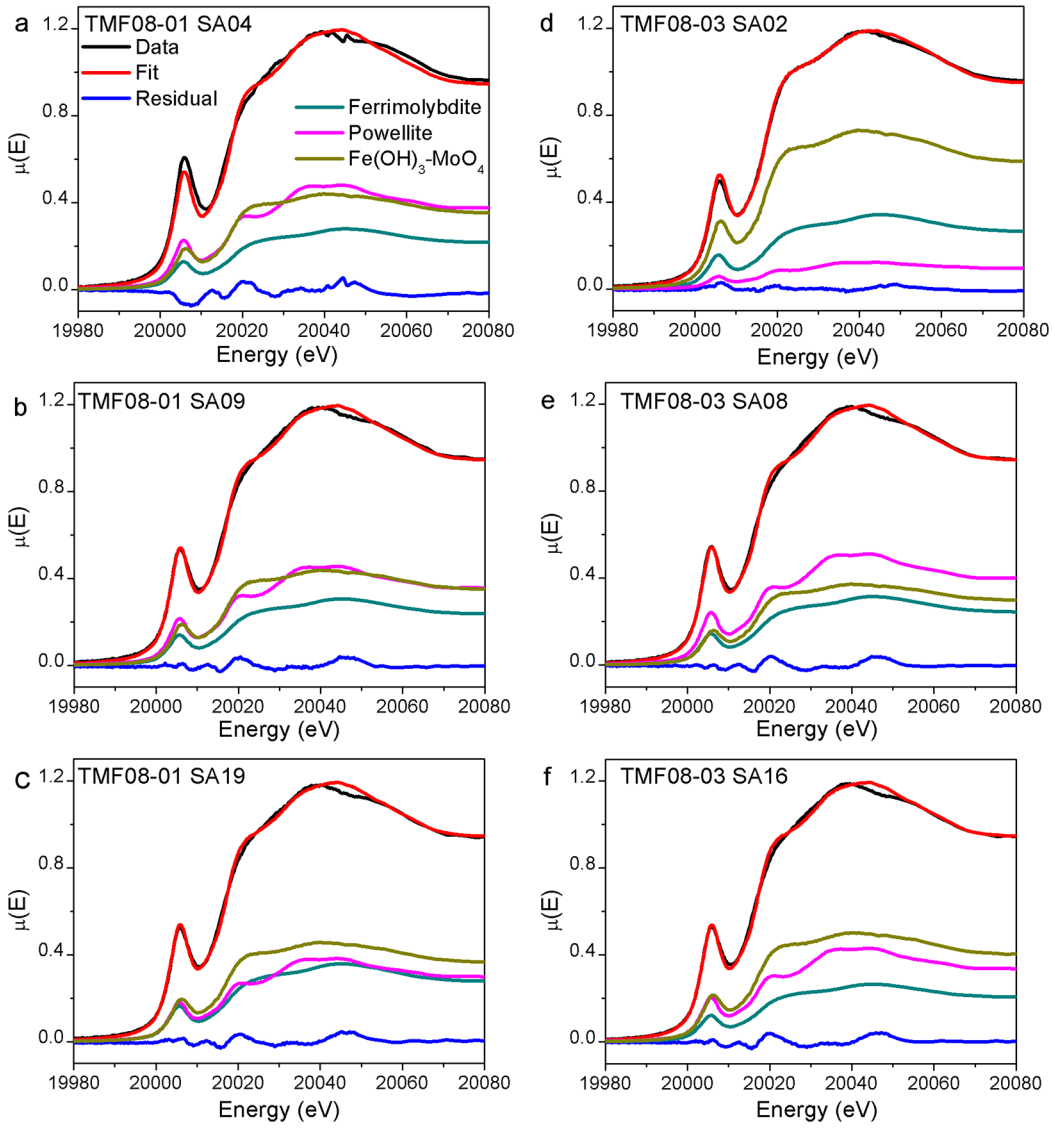

Figure 6. Mo K-edge XANES spectra from (a) TMF08-01 SA04, (b) TMF08-01 SA09, (c) TMF08-01 SA19, (d) TMF08-03 SA02, (e) TMF08-03 SA08, and (f) TMF08-03 SA16 are presented along with results of the linear combination fit. The weighted spectra from the fitted standards are also plotted.

Table 2. Summary of LCA Fits[a]

	powellite		ferrimolybdite		$Fe(OH)_3$–MoO_4			
sample	concentration	error	concentration	error	concentration	error	*R* factor	χ^2
TMF08-01 SA04	0.40	0.040	0.24	0.071	0.37	0.029	0.00466	0.16064
TMF08-01 SA09	0.38	0.022	0.26	0.038	0.36	0.017	0.00155	0.05318
TMF08-01 SA19	0.37	0.042	0.30	0.027	0.38	0.018	0.00178	0.06292
TMF08-03 SA02	0.10	0.033	0.29	0.014	0.600	0.0097	0.00052	0.01788
TMF08-03 SA08	0.42	0.038	0.26	0.027	0.31	0.018	0.00175	0.06185
TMF08-03 SA16	0.36	0.037	0.22	0.028	0.42	0.019	0.00191	0.06674

[a]Results of the linear combination fittings of the Mo K-edge spectra from the tailings samples. The best fits using powellite, ferrimolybdite, and $Fe(OH)_3$–MoO_4 are reported.

the reconstructions of the tailings spectra (see Figure S12 of the Supporting Information). It can be clearly seen in Figure S12 of the Supporting Information that no significant improvements are observed when reproducing the spectra with four versus three components, indicating that only three factors are necessary to describe the data.

3.3.3. Quantitative Analysis of Mo Speciation. The Mo K-edge spectra collected from the tailings samples can be compared to the Mo K-edge spectra from Mo-bearing standards to determine the speciation of Mo in the tailings samples. The standards used to fit the Mo K-edge spectra were H_2MoO_4, α-$FeMoO_4$, α-$NiMoO_4$, molybdate adsorbed on ferrhydrite [$Fe(OH)_3$–MoO_4], ferrimolybdite, and powellite.

dx.doi.org/10.1021/es404980x | Environ. Sci. Technol. 2014, 48, 4460–4467

The Mo K-edge spectra from these standards are presented in Figure 4b (the anhydrous ferrimolybdite standard used was an appropriate model system for hydrated ferrimolybdite given the local structural similarities around the Mo center in the two systems).

The tailings spectra were fitted by linear combinations of the XANES spectra from the standards using the linear combination fit function in the Athena software program.[19] Each tailings spectrum was fitted by all combinations of three or fewer standards, and the best fit was determined by the χ^2 value from these fittings. The coefficients of the linear combination fit were normalized and represent the concentrations of each species present as a function of total percent Mo. The best fits to the spectra are summarized in Table 2, and the fitted spectra are plotted in Figure 6.

In all cases, the spectra were fitted best using ferrimolybdite, powellite, and either H_2MoO_4 or $Fe(OH)_3$–MoO_4. The linear combination fits using either H_2MoO_4 or $Fe(OH)_3$–MoO_4 were generally of equal quality, likely because of the strong similarities between the spectra from H_2MoO_4 and $Fe(OH)_3$–MoO_4 (Figure 4b). Therefore, it is not possible to determine which of these species [H_2MoO_4 or $Fe(OH)_3$–MoO_4] is present by analysis of the XANES spectra alone. However, H_2MoO_4 is known to be highly soluble at the pH of the pore water present in the TMF (pH 7.3), and it therefore does not seem likely that this phase would be found as a solid in the JEB TMF.[30] This leads to the conclusion that the third component in these samples is $Fe(OH)_3$–MoO_4.

In general, the resulting fits accurately reproduce the collected spectra from the tailings samples, with the exception of the region between 20 040 and 20 050 eV, where the fitted spectra are consistently more intense than the experimental data. It is likely that multi-scattering resonances (MSRs) contribute significantly to the intensity of the features found in this region of the spectra.[31] In a MSR process, the core electron is excited to a continuum state and scatters multiple times off neighboring atoms, resulting in constructive and destructive interference of the photoelectron wave.[32] As such, these structures are highly dependent upon the crystal structure of the materials, and the intensity of MSR features will decrease as the crystallinity of the material decreases.[33] The XRD patterns show that the crystallinity of the phases present in the tailings samples vary widely and exhibit a high degree of disorder (cf. Figure 1 and Figure S1 of the Supporting Information). Therefore, it is highly likely that the Mo phases have only a low degree of crystallinity in the tailings samples, which would result in a muted MSR feature compared to the MSR feature observed in the Mo K-edge XANES spectra from the crystalline standards.

The interpretation reported here relies heavily on the assumption that the standards used in this analysis account for all of the Mo-bearing species in the sample. For example, the β-$NiMoO_4$ phase, which could not be successfully synthesized, represents a possible Mo species that was not included in the standards measured. In this species, Mo occupies a tetrahedral site, which would increase the intensity of the XANES spectrum in the pre-edge region (i.e., the ~20 000–20 010 eV energy range) compared to the pre-edge region from α-$NiMoO_4$, in which Mo occupies a six-coordinate site.[34] When fitting the spectra using α-$NiMoO_4$ as a component, the pre-edge was consistently under fitted, while the main edge was accurately reproduced. The statistics of these fits were poor compared to the statistics reported in Table 2, which lead to the conclusion that α-$NiMoO_4$ was not a component in the tailings samples. However, on the basis of the XRF results, which showed some correlation between the Ni and Mo signals, and the conditions under which the tailings are treated, which are similar to the reported β-$NiMoO_4$ synthetic conditions, it seems possible that β-$NiMoO_4$ could be present.[1,35,36] Notwithstanding, all fits that included α-$NiMoO_4$ also required a significant contribution from the powellite spectrum to reproduce the data. Therefore, on the basis of these fits, the conclusions regarding the presence of powellite remain valid.

These results show that powellite is present as a major component in the JEB TMF. They also show that ferrimolybdite and $Fe(OH)_3$–MoO_4 likely account for significant amounts of the Mo species present in the TMF. The conclusions of this study are consistent with the long-term geochemical models of the TMF, which predict that powellite will be the predominant Mo-bearing phase when the TMF reaches equilibrium.[7]

■ ASSOCIATED CONTENT

Supporting Information

Details of the synthetic procedures used, μ-XRD patterns, XRF maps, and results of the Laue diffraction indexing of the tailings samples studied and the principle factors calculated from the PCA and reconstructions of the measured Mo K-edge spectra from the tailings using the factors computed from the PCA. This material is available free of charge via the Internet at http://pubs.acs.org.

■ AUTHOR INFORMATION

Corresponding Author

*Telephone: 306-966-4660. Fax: 306-966-4730. E-mail: andrew.grosvenor@usask.ca.

Notes

The authors declare no competing financial interest.

■ ACKNOWLEDGMENTS

The Natural Sciences and Engineering Research Council of Canada (NSERC) supported this work through an Engage Grant awarded to Andrew P. Grosvenor. John R. Hayes also thanks the NSERC, the Government of Saskatchewan, and the University of Saskatchewan for financial support. The Canadian Foundation for Innovation (CFI) is thanked for providing funds to purchase the PANalytical Empyrean powder X-ray diffractometer used in this work. The authors extend their thanks to Dr. Renfei Feng and Darren Hunter for their help in carrying out measurements at the VESPERS beamline [07-B2-1, Canadian Light Source (CLS)] and Dr. Ning Chen and Dr. Weifeng Chen for their help in carrying out measurements using the HXMA beamline (06-ID1, CLS). M. R. Rafiuddin, E. R. Aluri, and J. D. S. Walker (Department of Chemistry, University of Saskatchewan) and B. Schmid (AREVA Resources Canada) are thanked for their contributions. Research described in this paper was performed at the CLS, which is funded by the CFI, the NSERC, the National Research Council (NRC), the Canadian Institutes of Health Research (CIHR), the Government of Saskatchewan, the Western Economic Diversification Canada, and the University of Saskatchewan.

REFERENCES

(1) Rowson, J.; Schmid, B. *Tailings Optimization and Validation Program*; AREVA Resources Canada: Saskatoon, Saskatchewan, Canada, 2011.

(2) Langmuir, D.; Mahoney, J.; MacDonald, A.; Rowson, J. Predicting arsenic concentrations in the porewaters of buried uranium mill tailings. *Geochim. Cosmochim. Acta* **1999**, *63*, 3379−3394.

(3) Langmuir, D.; Mahoney, J.; Rowson, J. Solubility products of amorphous ferric arsenate and crystalline scorodite ($FeAsO_4{\cdot}2H_2O$) and their application to arsenic behavior in buried mine tailings. *Geochim. Cosmochim. Acta* **2006**, *70*, 2942−2956.

(4) Mahoney, J.; Slaughter, M.; Langmuir, D.; Rowson, J. Control of As and Ni releases from a uranium mill tailings neutralization circuit: Solution chemistry, mineralogy and geochemical modeling of laboratory study results. *Appl. Geochem.* **2007**, *22*, 2758−2776.

(5) Chen, N.; Jiang, D. T.; Cutler, J.; Kotzer, T.; Jia, Y. F.; Demopoulos, G. P.; Rowson, J. W. Structural characterization of poorly-crystalline scorodite, iron(III)−arsenate co-precipitates and uranium mill neutralized raffinate solids using X-ray absorption fine structure spectroscopy. *Geochim. Cosmochim. Acta* **2009**, *73*, 3260−3276.

(6) Mahoney, J.; Langmuir, D.; Gosselin, N.; Rowson, J. Arsenic readily released to pore waters from buried mill tailings. *Appl. Geochem.* **2005**, *20*, 947−959.

(7) Mahoney, J. *Review of the Molybdenum Geochemistry in the JEB TMF*; AREVA Resources Canada: Saskatoon, Saskatchewan, Canada, 2010.

(8) Essilfie-Dughan, J.; Pickering, I. J.; Hendry, M. J.; George, G. N.; Kotzer, T. Molybdenum speciation in uranium mine tailings using X-ray absorption spectroscopy. *Environ. Sci. Technol.* **2011**, *45*, 455−460.

(9) Achary, S. N.; Patwe, S. J.; Mathews, M. D.; Tyagi, A. K. High temperature crystal chemistry and thermal expansion of synthetic powellite ($CaMoO_4$): A high temperature X-ray diffraction (HT-XRD) study. *J. Phys. Chem. Solids* **2006**, *67*, 774−781.

(10) Sleight, A. W.; Chamberland, B. L.; Weiher, J. F. Magnetic, Mossbauer, and structural studies on three modifications of $FeMoO_4$. *Inorg. Chem.* **1968**, *7*, 1094−1098.

(11) Otsuka, K.; Wang, Y.; Yamanaka, I.; Morikawa, A. Kinetic study of the partial oxidation of methane over $Fe_2(MoO_4)_3$ catalyst. *J. Chem. Soc., Faraday Trans.* **1993**, *89*, 4225−4230.

(12) Michel, F. M.; Ehm, L.; Liu, G.; Han, W. Q.; Antao, S. M.; Chupas, P. J.; Lee, P. L.; Knorr, K.; Eulert, H.; Kim, J.; Grey, C. P.; Celestian, A. J.; Gillow, J.; Schoonen, M. A. A.; Strongin, D. R.; Parise, J. B. Similarities in 2- and 6-line ferrihydrite based on pair distribution function analysis of X-ray total scattering. *Chem. Mater.* **2007**, *19*, 1489−1496.

(13) Kashiwabara, T.; Takahashi, Y.; Tanimizu, M. A XAFS study on the mechanism of isotopic fractionation of molybdenum during its adsorption on ferromanganese oxides. *Geochem. J.* **2009**, *43*, e31−e36.

(14) Kraus, W.; Nolze, G. POWDER CELL—A program for the representation and manipulation of crystal structures and calculation of the resulting X-ray powder patterns. *J. Appl. Crystallogr.* **1996**, *29*, 301−303.

(15) Tamura, N.; MacDowell, A. A.; Spolenak, R.; Valek, B. C.; Bravman, J. C.; Brown, W. L.; Celestre, R. S.; Padmore, H. A.; Batterman, B. W.; Patal, J. R. Scanning X-ray microdiffraction with submicrometer white beam for strain/stress and orientation mapping in thin films. *J. Synchrotron Radiat.* **2003**, *10*, 137−143.

(16) Webb, S. M. The MicroAnalysis Toolkit: X-ray fluorescence image processing software. *AIP Conf. Proc.* **2011**, *196*, 196−199.

(17) Jiang, D. T.; Chen, N.; Zhang, L.; Malgorzata, G.; Wright, G. XAFS at the Canadian Light Source. *AIP Conf. Proc.* **2007**, *882*, 893.

(18) Thompson, A.; Attwood, D.; Gullikson, E.; Howells, M.; Kim, K.-J.; Kirz, J.; Kortright, J.; Lindau, I.; Pianetta, P.; Robinson, A.; Scofield, J.; Underwood, J.; Vaughn, D.; Williams, G.; Winick, H. *X-Ray Data Booklet*; Lawrence Berkeley National Laboratory: Berkeley, CA, 2009.

(19) Ravel, B.; Newville, M. ATHENA, ARTEMIS, HEPHAESTUS: Data analysis for X-ray absorption spectroscopy using IFEFFIT. *J. Synchrotron Radiat.* **2005**, *12*, 537−541.

(20) Pecharsky, V. K.; Zavalij, P. Y. *Fundamentals of Powder Diffraction and Structural Characterization of Materials*, 2nd ed.; Springer US: Boston, MA, 2009.

(21) Smith, D. K. Crystallite statistics and accuracy in powder diffraction intensity measurements. In *Defect and Microstructure Analysis*; Snyder, R. L., Fiala, J., Bunge, H. J., Eds.; Oxford University Press: Oxford, U.K., 1999; pp 333−345.

(22) Rindby, A.; Engström, P.; Janssens, K. The use of a scanning X-ray microprobe for simultaneous XRF/XRD studies of fly-ash particles. *J. Synchrotron Radiat.* **1997**, *4*, 228−235.

(23) Gaultois, M. W.; Grosvenor, A. P. Coordination-induced shifts of absorption and binding energies in the $SrFe_{1-x}Zn_xO_{3-\delta}$ system. *J. Phys. Chem. C* **2010**, *114*, 19822−19829.

(24) Farges, F.; Siewert, R.; Brown, G. E.; Guesdon, A.; Morin, G. Structural environments around molybdenum in silicate glasses and melts. I. Influence of composition and oxygen fugacity on the local structure of molybdenum. *Can. Miner.* **2006**, *44*, 731−753.

(25) Karppinen, M.; Fukuoka, A.; Niinistö, L.; Yamauchi, H. Determination of oxygen content and metal valences in oxide superconductors by chemical methods. *Supercond. Sci. Technol.* **1996**, *9*, 121−135.

(26) Atkins, P.; Overton, T.; Rourke, J.; Weller, M.; Armstrong, F. *Inorganic Chemistry*, 4th ed.; Oxford University Press: Oxford, U.K., 2006; pp 774−785.

(27) Fernández-García, M.; Márquez Alvarez, C.; Haller, G. L. XANES−TPR study of Cu−Pd bimetallic catalysts: Application of factor analysis. *J. Phys. Chem.* **1995**, *99*, 12565−12569.

(28) Malinowski, E. R. *Factor Analysis in Chemistry*, 3rd ed.; John Wiley and Sons: Hoboken, NJ, 2002.

(29) Malinowski, E. R. Theory of error in factor analysis. *Anal. Chem.* **1977**, *49*, 606−612.

(30) Frey, R. Personal communication; AREVA Resources Canada: Saskatoon, Saskatchewan, Canada, 2013.

(31) Herrero-Martín, J.; García, J.; Subías, G.; Blasco, J.; Sánchez, M. C. An X-ray spectroscopic study of A_2FeMoO_6 and $Sr_2Fe_{1-x}Cr_xO_6$ double perovskites. *J. Phys.: Condens. Matter* **2004**, *16*, 6877−6890.

(32) Rehr, J. J.; Albers, R. C. Theoretical approaches to X-ray absorption fine structure. *Rev. Mod. Phys.* **2000**, *72*, 621−654.

(33) Huguenin, F.; Ticianelli, E. A.; Torresi, R. M. XANES study of polyaniline−V_2O_5 and sulfonated polyaniline−V_2O_5 nanocomposites. *Electrochim. Acta* **2002**, *47*, 3179−3186.

(34) Rodriguez, J. A.; Hanson, J. C.; Chaturvedi, S.; Maiti, A.; Brito, J. L. Phase transformations and electronic properties in mixed-metal oxides: Experimental and theoretical studies on the behavior of $NiMoO_4$ and $MgMoO_4$. *J. Chem. Phys.* **2000**, *112*, 935.

(35) Brito, J. L.; Barbosa, A. L. Effect of phase composition of the oxidic precursor on the HDS activity of the sulfided molybdates of Fe(II), Co(II), and Ni(II). *J. Catal.* **1997**, *171*, 467−475.

(36) Mazzocchia, C.; Aboumrad, C.; Diagne, C.; Tempesti, E.; Herrmann, J. M.; Thomas, G. On the $NiMoO_4$ oxidative dehydrogenation of propane to propene: Some physical correlations with the catalytic activity. *Catal. Lett.* **1991**, *10*, 181−192.